

Elastocaloric Response of PbTiO₃ Predicted from a First-Principles Effective Hamiltonian

Jordan A. Barr¹, Scott P. Beckman¹, and Takeshi Nishimatsu^{2*}

¹*Department of Materials Science and Engineering, Iowa State University, Ames, Iowa 50011, USA*

²*Institute for Materials Research (IMR), Tohoku University, Sendai 980-8577, Japan*

A first-principles effective Hamiltonian is used in a molecular dynamics simulation to study the elastocaloric effect in PbTiO₃. It is found that the transition temperature is a linear function of uniaxial tensile stress. A negative temperature change is calculated, when the uniaxial tensile stress is switched off, as a function of the initial temperature $\Delta T(T_{\text{initial}})$. It is predicted that the formation of domain structures under uniaxial tensile stress degrades the effectiveness of the elastocaloric effect.

1. Introduction

Solid-state caloric effects provide a promising approach to future refrigeration technologies. The electrocaloric,^{1–4} magnetocaloric,^{5,6} and barocaloric effects^{7,8} produce a temperature change due to entropic changes induced by the application of an electric field, magnetic field, and pressure, respectively. The application of uniaxial stress to a ferroelectric material affects the spontaneous polarization and produces an adiabatic temperature change. This is called the elastocaloric effect.^{9–13}

Here, a first-principles effective Hamiltonian model implemented within a molecular dynamics (MD) framework is used to predict the elastocaloric response of PbTiO₃. Following the work of Lisenkov *et al.*,¹¹ the elastocaloric response of PbTiO₃ is examined for tensile uniaxial loads ranging from 0 to –2.0 GPa and temperatures ranging from 300 to 1000 K. The results of this study will be compared with those reported in the literature.

2. Methods

The effective Hamiltonian used is

$$\begin{aligned}
 H^{\text{eff}} = & \frac{M_{\text{dipole}}^*}{2} \sum_{\mathbf{R}, \alpha} \dot{u}_{\alpha}^2(\mathbf{R}) + \frac{M_{\text{acoustic}}^*}{2} \sum_{\mathbf{R}, \alpha} \dot{w}_{\alpha}^2(\mathbf{R}) \\
 & + V^{\text{self}}(\{\mathbf{u}\}) + V^{\text{dpl}}(\{\mathbf{u}\}) + V^{\text{short}}(\{\mathbf{u}\}) \\
 & + V^{\text{elas, homo}}(\eta_1, \dots, \eta_6) + V^{\text{elas, inho}}(\{\mathbf{w}\}) \\
 & + V^{\text{coup, homo}}(\{\mathbf{u}\}, \eta_1, \dots, \eta_6) + V^{\text{coup, inho}}(\{\mathbf{u}\}, \{\mathbf{w}\}).
 \end{aligned} \tag{1}$$

Here, the collective atomic motion is coarse-grained by the local soft mode vectors $\mathbf{u}(\mathbf{R})$ and local acoustic displacement vectors $\mathbf{w}(\mathbf{R})$ of each unit cell at \mathbf{R} in a simulation supercell. η_1, \dots, η_6 are the six components of homogeneous strain in Voigt notation. $\frac{M_{\text{dipole}}^*}{2} \sum_{\mathbf{R}, \alpha} \dot{u}_{\alpha}^2(\mathbf{R})$ and $\frac{M_{\text{acoustic}}^*}{2} \sum_{\mathbf{R}, \alpha} \dot{w}_{\alpha}^2(\mathbf{R})$ are the kinetic energies possessed by the local soft modes and local acoustic displacement vectors along with their effective masses of M_{dipole}^* and M_{acoustic}^* ; $V^{\text{self}}(\{\mathbf{u}\})$ is the local-mode self-energy, $V^{\text{dpl}}(\{\mathbf{u}\})$ is

the long-range dipole-dipole interaction, $V^{\text{short}}(\{\mathbf{u}\})$ is the short-range interaction between local soft modes, $V^{\text{elas, homo}}(\eta_1, \dots, \eta_6)$ is the elastic energy from homogeneous strains, $V^{\text{elas, inho}}(\{\mathbf{w}\})$ is the elastic energy from inhomogeneous strains, $V^{\text{coup, homo}}(\{\mathbf{u}\}, \eta_1, \dots, \eta_6)$ is the coupling between the local soft modes and the homogeneous strain, and $V^{\text{coup, inho}}(\{\mathbf{u}\}, \{\mathbf{w}\})$ is the coupling between the soft modes and the inhomogeneous strains. Details of this Hamiltonian are explained in Refs. 14–16. Additionally, to investigate the effects from stress, we use the enthalpy $\mathcal{H} = H^{\text{eff}} + Na_0^3 \boldsymbol{\sigma} \cdot \boldsymbol{\eta}$, where $N = L_x \times L_y \times L_z$ is the supercell size and a_0 is the unit cell length; therefore, Na_0^3 is the supercell volume and $\boldsymbol{\sigma}$ is the six components of stress. In this study, we apply uniaxial tensile stress to the system along the z -direction. It is implemented in the MD framework, and the MD simulation program is called **feram**. **feram** is distributed as free software under the conditions described in the GNU General Public License from its website.¹⁷ Examples of the input files are packaged within the source code under the **feram-0.22.05/src/28example-PbTiO3-elastocaloric-770K/** directory. The model parameters for PbTiO₃ are determined semi-empirically in a previous work¹⁸ and adopted for **feram** in Ref. 19.

Using the above parameters, the results of heating-up and cooling-down test MD simulations for a supercell of $N = 16 \times 16 \times 16$ are shown in Fig. 1. From the temperature T dependences of the averaged lattice constants [shown in Fig. 1(a)], a tetragonal-to-cubic ferroelectric-to-paraelectric phase transition is clearly observed upon heating-up to 672 K. During the cooling-down simulation, 90° ferroelectric domains are formed at 630 K and are frozen at a low temperature, as described in Ref. 19. These two transition temperatures are largely dependent on supercell size with a slight dependence on the initial random configurations of $\{\mathbf{u}\}$. However, their average of 653 K is in good agreement with those obtained in earlier Monte Carlo¹⁸ and MD¹⁹ simulations, in which the same set of parameters were used. This is lower than the experimental value $T_C = 763$ K.²⁰ This disagreement between simulations and experiments is unavoidable, owing to the errors in the total energy of the first-principles

*E-mail: t-nissie@imr.tohoku.ac.jp

calculations, which is around 10 meV per unit cell. In Fig. 1(b), the temperature dependence of the total energy per unit cell is plotted for heating-up and cooling-down test simulations. At the transition temperatures, we observe jumps in the total energy, i.e., the latent heat. In Figs. 1(c) and 1(d), the relative dielectric constant tensor computed from the fluctuations of the dipoles is plotted. This is defined as

$$\epsilon_{\alpha\beta} = \frac{1}{V\epsilon_0 k_B T} [\langle p_\alpha p_\beta \rangle - \langle p_\alpha \rangle \langle p_\beta \rangle], \quad (2)$$

where V is the volume of the supercell, ϵ_0 is the absolute dielectric constant of vacuum, k_B is the Boltzmann constant, p_α is the $\alpha (= x, y, z)$ component of the total electric dipole moment in the supercell, $\mathbf{p} = Z^* \sum_{\mathbf{R}} \mathbf{u}(\mathbf{R})$, Z^* is the Born effective charge associated with a soft mode vector, and the angle brackets $\langle \rangle$ denote the statistical time average.²¹ Divergence in the dielectric constants at the transition temperatures can be clearly observed, although it is slightly underestimated compared with the experimentally observed value.²²

Temperature-independent elastic coefficients ($C_{11} = 302$ GPa, $C_{12} = 132$ GPa, $C_{44} = 351$ GPa) determined from the cubic structure are used, although they slightly depend on temperature even with this Hamiltonian of Eq. (1) because strains η_1, \dots, η_6 and dipoles $\{\mathbf{u}\}$ couple through $V^{\text{coup, homo}}(\{\mathbf{u}\}, \eta_1, \dots, \eta_6)$.

As shown in Fig. 2, the simulation procedure for determining the elastocaloric response of PbTiO_3 is similar to that used for the “direct” prediction of the electrocaloric effect presented in Ref. 23. A supercell size of $N = 64 \times 64 \times 64$ is used and is thermalized for 50,000 time steps in a canonical ensemble at the constant initial temperature T_{initial} and constant applied stress. A single-domain $+z$ -polarized initial configuration for the first thermalization MD is generated randomly with certain averages and deviations for $\{\mathbf{u}\}$: $\langle u_x \rangle = \langle u_y \rangle = 0$, $\langle u_z \rangle = 0.33 \text{ \AA}$, $\langle u_x^2 \rangle - \langle u_x \rangle^2 = \langle u_y^2 \rangle - \langle u_y \rangle^2 = (0.045 \text{ \AA})^2$, and $\langle u_z^2 \rangle - \langle u_z \rangle^2 = (0.021 \text{ \AA})^2$. Once thermalized, the system is switched from being held at a constant temperature to being isolated as a microcanonical ensemble. The mechanical load is removed and the system is allowed to equilibrate for 40,000 time steps. Once equilibrated, the system’s final temperature T_{final} is determined by averaging the acoustic and dipole kinetic energies for 10,000 time steps. The time step for this simulation is 2 fs. One of the advantages of this “direct” prediction method is that the temperature and external-field dependences of heat capacity and latent heat are implicitly and automatically included in the simulations, whereas in the “indirect” method, an experimentally observed heat capacity must be used in the entire temperature and external field ranges, as described in Ref. 24. The temperature ranges from 300 to 1000 K, incremented with a step size of 1 K, and the applied uniaxial stress ranges from 0 to -2.0 GPa, incremented with a step size of -0.2 GPa.

3. Results and Discussion

The elastocaloric response $\Delta T_{\text{raw}} = T_{\text{final}} - T_{\text{initial}}$ of PbTiO_3 is presented in Fig. 3(a). Scaling from ΔT_{raw} to $\Delta T_{\text{corrected}} = \frac{2}{5} \Delta T_{\text{raw}}$ must be employed to account for

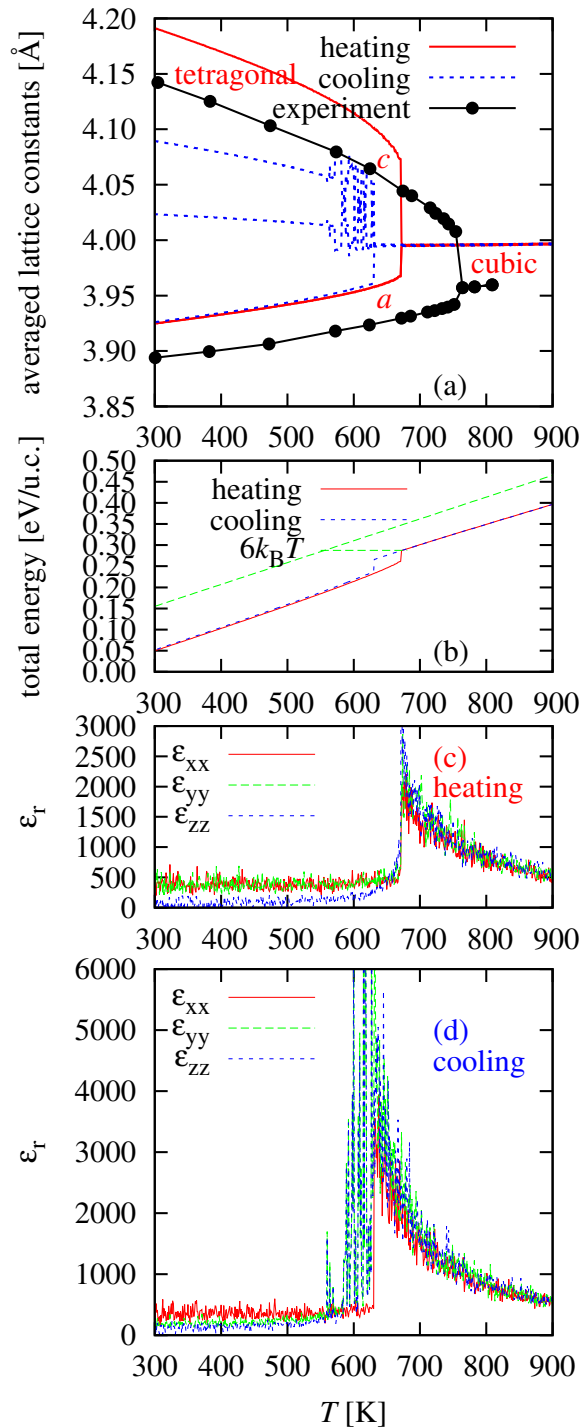


Fig. 1. (Color online) Heating-up and cooling-down MD simulations of bulk PbTiO_3 . (a) Averaged lattice constants. (b) Total energy per unit cell. Three components of relative dielectric constant are also plotted for (c) heating-up and (d) cooling-down simulations. Thermal hysteresis can be seen. In (a), experimentally observed lattice constants²⁰ are plotted with black solid lines.

the reduced degrees of freedom due to coarse graining, as discussed in Ref. 23. In Fig. 3(b), polarizations along the z -direction before and after the release of the load of $\sigma_3 = -1.6$ GPa are compared, i.e., $P_z(T_{\text{initial}}, \sigma_3 = -1.6 \text{ GPa})$ and $P_z(T_{\text{final}}, \sigma_3 = 0)$ are compared, respectively. We redefine the transition temperature under uni-

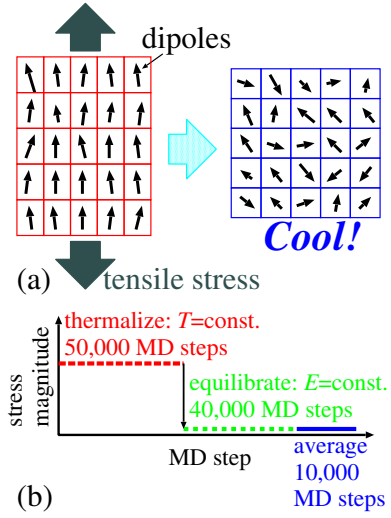


Fig. 2. (Color online) (a) Schematic illustration of elastocaloric cooling. (b) Procedure of direct simulation of the elastocaloric effect.

axial stress as $T'_C(\sigma_3)$. For $\sigma_3 = -1.6$ GPa, $T'_C = 917$ K. Transformation from T'_C is indicated with a dashed blue arrow. Above a certain temperature (T_{onset}), there is a temperature range $T_{\text{onset}} < T_{\text{initial}} \leq T'_C$ in which one can obtain a large elastocaloric effect. Transformation from T_{onset} is indicated by a dotted magenta arrow. It can be seen that below T_{onset} ($T_{\text{initial}} \leq T_{\text{onset}}$), transformation from switching off the uniaxial tensile stress is from an elongated ferroelectric polarized state to a normal ferroelectric polarized state. Between T_{onset} and T'_C , i.e., $T_{\text{onset}} < T_{\text{initial}} \leq T'_C$, the transformation changes from a stress-enhanced ferroelectric polarized state to a paraelectric nonpolar state, resulting in a large elastocaloric response. Just above T_{onset} , a maximum $|\Delta T|$ is obtained and its transformation is indicated by a solid red arrow in Fig. 3(b). Above T'_C ($T'_C < T_{\text{initial}}$), even under the uniaxial tensile stress load, the system remains paraelectric and consequently $|\Delta T| = 0$.

In Figs. 3(c)–3(e), $P_z(T_{\text{initial}}, \sigma_3 \leq 0)$ and $P_z(T_{\text{final}}, \sigma_3 = 0)$ are plotted also for loads of $\sigma_3 = -0.8$, -0.4 , and 0.0 GPa. In Fig. 3(c), it is observed that with a load of -0.8 GPa, the effective temperature range $T_{\text{onset}} < T_{\text{initial}} \leq T'_C$ becomes narrower than that of -1.6 GPa. In Fig. 3(d), it can be seen that the initial uniaxial tensile load of -0.4 GPa is not sufficiently large to induce a ferroelectric-to-paraelectric transformation. Therefore, we cannot define T_{onset} for loads of $0.0 < \sigma_3 < -0.4$ GPa. In the case of zero load, in Fig. 3(e), the accuracy of our MD simulations ($\Delta T \equiv 0$) and the simulated and underestimated phase transition temperature of $T'_C = 640$ K under zero pressure are shown. As anticipated, the greater the uniaxial loading, the greater the induced temperature change $|\Delta T|$, and for a loading of -2.0 GPa, a temperature change of -43 K is predicted.

In Fig. 4, plots show $\max|\Delta T_{\text{corrected}}|$, and T_{onset} and T'_C under different applied loads. It can be seen that T'_C linearly depends on applied load. T_{onset} depends on applied load nearly linearly in $-0.6 < \sigma_3 < -2.0$, but less

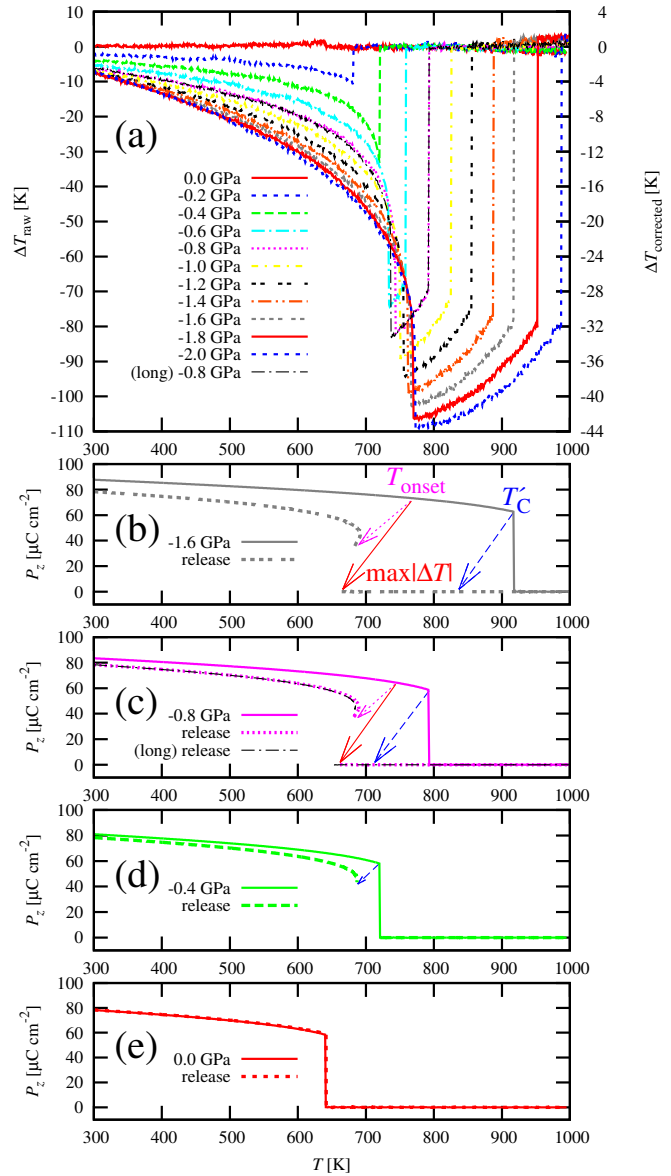


Fig. 3. (Color online) (a) Simulated elastocaloric effect (ΔT) in PbTiO_3 as a function of initial temperature (T_{initial}). The applied uniaxial stress ranges from 0 to -2.0 GPa. ΔT is scaled from ΔT_{raw} to $\Delta T_{\text{corrected}}$ by accounting for the reduced degrees of freedom, as discussed in Ref. 23. (b) Polarization along the z -axis both before [$P_z(T_{\text{initial}})$] (gray solid line) and after [$P_z(T_{\text{final}})$] (gray dotted line) the release of load of -1.6 GPa. (c) $P_z(T_{\text{initial}})$ (cyan solid line) and $P_z(T_{\text{final}})$ (cyan dotted line) of load of -0.8 GPa. $P_z(T_{\text{final}})$ after 990,000 MD time steps (thin black chain line). (d) $P_z(T_{\text{initial}})$ (green solid line) and $P_z(T_{\text{final}})$ (green dashed line) of load of -0.4 GPa. (e) $P_z(T_{\text{initial}})$ (green solid line) and $P_z(T_{\text{final}})$ (green dashed line) of zero load. In (b)–(d), transformations that give T_{onset} , $\max|\Delta T|$, and T'_C are indicated by dotted magenta, solid red, and dashed blue arrows, respectively.

steeply than T'_C .

T_{onset} is also found to depend on the period of equilibration. Between T_C and T_{onset} ($T_C < T_{\text{initial}} \leq T_{\text{onset}}$), when a uniaxial tensile stress is applied and then released, the system stays in a ferroelectric state and does not transform into a paraelectric state. In other words, the system *remembers* the strength of the stress applied. This is confirmed with a longer equilibration of 990,000 time steps instead of the 40,000 shown in Fig. 2. As in-

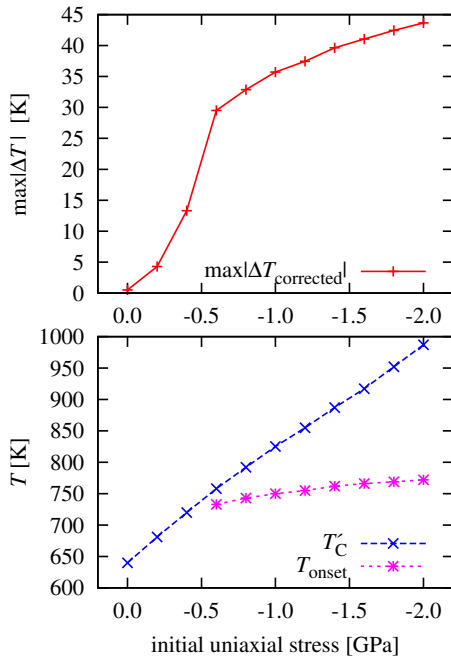


Fig. 4. (Color online) Plots of $\max|\Delta T_{\text{corrected}}|$, T_{onset} , and T'_C vs the different initially applied uniaxial tensile stresses. Data are connected with solid red, dotted magenta, and dashed blue lines, respectively.

indicated by black chain lines in Figs. 3(a) and 3(c), T_{onset} with longer equilibration becomes 736 K, whereas that of 40,000 was 744 K, i.e., the system *forgets* the strength of the stress applied. Therefore, the stronger load and the shorter period of equilibration result in a higher T_{onset} .

In Contrast, in Fig. 5, we also perform “heating” simulations with switching-on of uniaxial stress in which the system is firstly thermalized under zero stress and then ΔT is measured under switched-on uniaxial tensile stresses. Zigzag structures at the final temperatures are observed. A vertical cross section and a horizontal slice of a final state indicated by a “+” mark in Fig. 5 are shown in Figs. 6 and 7, respectively. The supercell is divided into the $+z$ and $-z$ domains. It can be understood that the zigzag structures arise from the existence and nonexistence of domain structures. In the elastocaloric effect, domain structures may be formed more easily than in the electrocaloric effect, because there is no significant $+z$ - or $-z$ -direction in the uniaxial stress, but there is in the external electric field. It is suggested that the formation of domain structures may cause some degradations in effectiveness in applications of the elastocaloric effect. Note also that when comparing Figs. 3(a) and 5, the onset temperature is constant in switching-on “heating” simulations because the simulations are started from zero stress.

The results presented here can be compared with those presented by Lisenkov *et al.* in their Fig. 1(b).¹¹ Note that their ΔT is positive because they switched on the uniaxial stress from zero stress. For the same reason, their onset initial temperature, which gives $\max|\Delta T|$, is always T_C . We have carried out *switching-off* time-dependent MD simulations and found the applied-stress

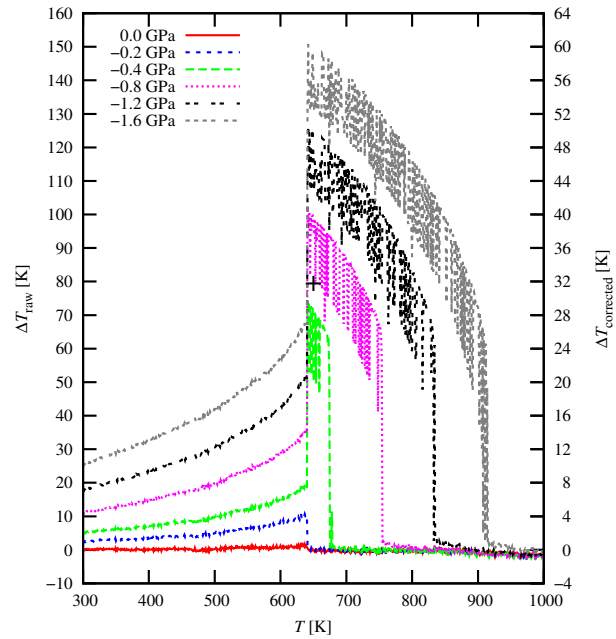


Fig. 5. (Color online) Simulated switching-on elastocaloric effect with positive ΔT in PbTiO_3 as functions of initial temperature, T_{initial} . The switched-on uniaxial stress ranges from 0 to -1.6 GPa. ΔT is scaled from ΔT_{raw} to $\Delta T_{\text{corrected}}$. Zigzag structures in final temperatures are observed. A vertical cross section and a horizontal slice of a final state indicated with a “+” mark for a -0.8 GPa simulation are shown in Figs. 6 and 7, respectively.

and equilibration-period dependences of T_{onset} because we consider that hysteretic behavior is important for the cooling application of the elastocaloric effect.

Furthermore, whereas Lisenkov *et al.* reported a continuous linear increase in $\max|\Delta T|$ as stronger stresses are applied and a maximum of approximately $+35$ K for a tensile load of -2.0 GPa, our results of initial stress dependence of $\max|\Delta T|$ are not continuous at around -0.5 GPa. Our MD simulation for a tensile load of -2.0 GPa results in $\max|\Delta T_{\text{corrected}}| = |-43|$ K.

Finally, the shapes of the two ΔT vs T plots differ in the high-temperature regime. Both models have a $\max|\Delta T|$ that increases with loading, but the results here show a sharper drop in $|\Delta T|$ at T'_C , although this difference might be due to differences in the implementations, not the underlying physics. In Fig. 4, it is observed that T'_C increases linearly with increased loading to a temperature of 1000 K, and presumably above, whereas Ref. 11 states that the elastocaloric response disappears for temperatures above 890 K.

4. Summary

Note that these simulations are very ideal and unrealistic ones. For example, applying such huge tensile uniaxial stresses is difficult and the phase transition of pure PbTiO_3 would cause cracks in a crystal experimentally. However, these ideal simulations suggest that, for example, elastocaloric cooling has the largest effect when a ferroelectric-to-paraelectric phase transition occurs.

In summary, a first-principles effective Hamiltonian is used in a molecular dynamics simulation to study the elastocaloric effect in PbTiO_3 . The results show that for a

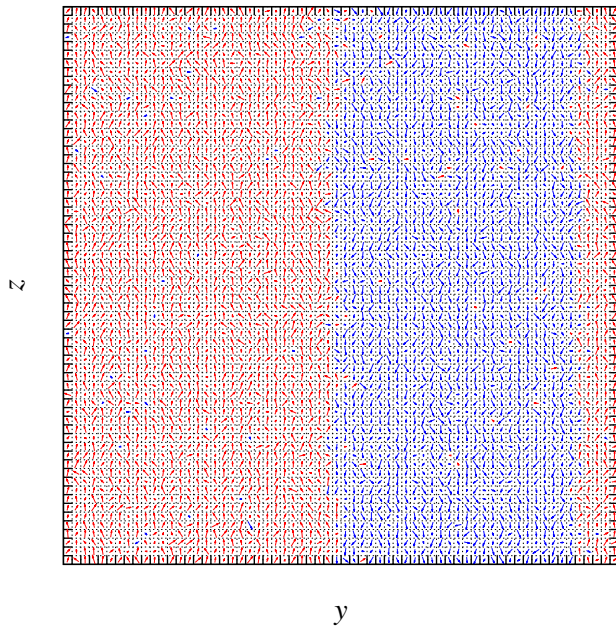


Fig. 6. (Color online) Vertical cross section of a final state indicated with a “+” mark in Fig. 5. Dipole moments of each site are projected onto the yz -plane and indicated with arrows. The arrows are colored with red or blue if each dipole has $+z$ or $-z$ component, respectively.

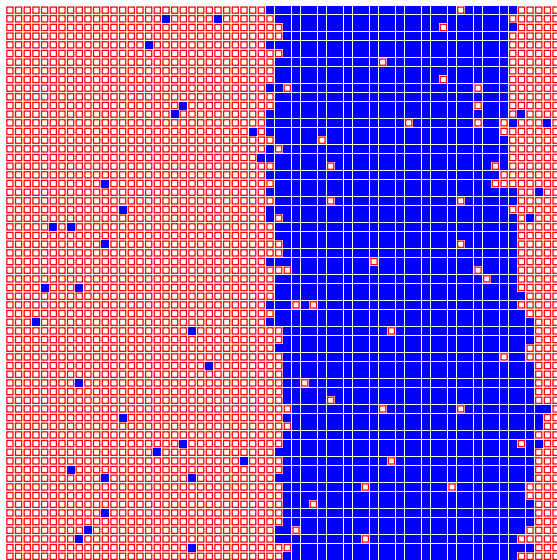


Fig. 7. (Color online) Horizontal slice of a final state indicated with a “+” mark in Fig. 5. $+z$ -polarized and $-z$ -polarized sites are denoted by red \square and blue \blacksquare , respectively.

modest loading of around -0.5 GPa, a thermal response of around -25 K can be achieved, but for a large load of around -2.0 GPa, the thermal response can be as large as -44 K.

The onset temperature T_{onset} and the termination temperature, T'_C , are identified as the temperatures bracketing the temperature range where the elastocaloric effect is greatest. T'_C is found to scale linearly with initial load, whereas T_{onset} has a less steep linearity. Although increasing the initial stress widens the window of temper-

atures continuously, the initial stress dependence of ΔT becomes smaller for stresses stronger than -0.5 GPa.

The formation of domain structures is observed in switching-on “heating” simulations and it is suggested that the formation of domain structures may cause some malfunctions in applications of the elastocaloric effect.

The results here are in qualitative agreement with those reported in Ref. 11, which were prepared using an effective Hamiltonian in a Monte Carlo model; however, there are physically significant differences including temperature and applied-stress dependences of ΔT . There is no easy explanation for these differences, and this requires future investigation.

Acknowledgments

The work of JAB and SPB was supported by the US National Science Foundation (NSF) through grant No. DMR-1105641. The NSF acknowledged for sponsoring JAB’s travel to Tohoku University, which was provided through grant No. DMR-1037898. The work of TN was supported in part by JSPS KAKENHI Grant Number 25400314. This work was also supported in part by the Strategic Programs for Innovative Research (SPIRE), MEXT, and the Computational Materials Science Initiative (CMSI), Japan. The computational resources were provided by the Center for Computational Materials Science, Institute for Materials Research (CCMS-IMR), Tohoku University. We thank the staff at CCMS-IMR for their constant effort. This research was also conducted using the Fujitsu PRIMEHPC FX10 System (Oakleaf-FX, Oakbridge-FX) in the Information Technology Center, The University of Tokyo.

- 1) G. G. Wiseman and J. K. Kuebler, *Phys. Rev.* **131**, 2023 (1963).
- 2) J. Scott, *Annu. Rev. Mater. Res.* **41**, 229 (2011).
- 3) H. Gränicher, *Helv. Phys. Acta* **29**, 210 (1956).
- 4) E. Hegenbarth, *Cryogenics* **1**, 242 (1961).
- 5) K. A. Gschneidner Jr., V. K. Pecharsky, and A. O. Tsokol, *Rep. Prog. Phys.* **68**, 1479 (2005).
- 6) E. Warburg, *Ann. Phys. (Berlin)* **249**, 141 (1881).
- 7) L. Mañosa, D. González-Alonso, A. Planes, E. Bonnot, M. Barrio, J.-L. Tamarit, S. Aksoy, and M. Acet, *Nat. Mater.* **9**, 478 (2010).
- 8) M. Gorev, E. Bogdanov, I. Flerov, and N. Laptash, *J. Phys.: Condens. Matter* **22**, 185901 (2010).
- 9) P. O. Castillo-Villa, L. Mañosa, A. Planes, D. E. Soto-Parra, J. Sánchez-Llamazares, H. Flores-Zúñiga, and C. Frontera, *J. Appl. Phys.* **113**, 053506 (2013).
- 10) S. Lisenkov and I. Ponomareva, *Phys. Rev. B* **86**, 104103 (2012).
- 11) S. Lisenkov, B. K. Mani, C.-M. Chang, J. Almand, and I. Ponomareva, *Phys. Rev. B* **87**, 224101 (2013).
- 12) J. Cui, Y. Wu, J. Muehlbauer, Y. Hwang, R. Radermacher, S. Fackler, M. Wuttig, and I. Takeuchi, *Appl. Phys. Lett.* **101**, 073904 (2012).
- 13) E. Bonnot, R. Romero, L. Mañosa, E. Vives, and A. Planes, *Phys. Rev. Lett.* **100**, 125901 (2008).
- 14) R. D. King-Smith and D. Vanderbilt, *Phys. Rev. B* **49**, 5828 (1994).
- 15) W. Zhong, D. Vanderbilt, and K. M. Rabe, *Phys. Rev. B* **52**, 6301 (1995).
- 16) T. Nishimatsu, U. V. Waghmare, Y. Kawazoe, and D. Vanderbilt, *Phys. Rev. B* **78**, 104104 (2008).

- 17) T. Nishimatsu, feram at SourceForge.net, <http://loto.sourceforge.net/feram/>, 2007-2014.
- 18) U. V. Waghmare and K. M. Rabe, Phys. Rev. B **55**, 6161 (1997).
- 19) T. Nishimatsu, K. Aoyagi, T. Kiguchi, T. J. Konno, Y. Kawazoe, H. Funakubo, A. Kumar, and U. V. Waghmare, J. Phys. Soc. Jpn. **81**, 124702 (2012).
- 20) G. Shirane, S. Hoshino, and K. Suzuki, Phys. Rev. **80**, 1105 (1950).
- 21) L. Bellaiche, J. Íñiguez, E. Cockayne, and B. P. Burton, Phys. Rev. B **75**, 014111 (2007).
- 22) J. Remeika and A. Glass, Materials Research Bulletin **5**, 37 (1970).
- 23) T. Nishimatsu, J. A. Barr, and S. P. Beckman, J. Phys. Soc. Jpn. **82**, 114605 (2013).
- 24) S. P. Beckman, L. F. Wan, J. A. Barr, and T. Nishimatsu, Mater. Lett. **89**, 254 (2012).